Multifractal analysis of stack voltage based on wavelet leaders: A new tool for PEMFC diagnosis

Djedjiga Benouioua, Denis Candusso, Fabien Harel, Latifa Oukhellou

Multifractal Analysis of Stack Voltage Based on Wavelet Leaders: A New Tool for PEMFC Diagnosis

Djedjiga Benouioua[1,2,3], Denis Candusso[1,2,3], Fabien Harel[3,4], Latifa Oukhellou[5]
[1] ITE EFFICACITY, 14-20 boulevard Newton, Champs-sur-Marne, F-77447 Marne la Vallée, France.
[2] IFSTTAR / COSYS / SATIE (UMR CNRS 8029), 25 Allée des marronniers, F-78000 Versailles Satory, France.
[3] FC LAB (FR CNRS 3539), UTBM Bât. F, Rue Thierry Mieg, F-90010 Belfort Cedex, France.
[4] Université de Lyon, IFSTTAR / AME / LTE, 25 Avenue François Mitterrand, Case24, Cité des mobilités, F-69675 Bron Cedex, France.
[5] Université Paris Est, IFSTTAR / COSYS / GRETTIA, 14-20 Boulevard Newton, Cité Descartes, Champs sur Marne, F-77447 Marne la Vallée Cedex 2, France

djedjiga.benouioua@ifsttar.fr, denis.candusso@ifsttar.fr, fabien.harel@ifsttar.fr, latifa.oukhellou@ifsttar.fr

Abstract
To achieve a fast and low cost diagnostic, we propose a new tool based on wavelet leaders in which the PEMFC diagnosis is made by the observation of the one and only stack voltage. The steps of our strategy are the following ones:
- The PEMFC is operated under a variety of conditions (nominal or severe) using a characterization testbench developed in lab. The severe operating conditions refer either to single fault types or to different combinations of faults.
- The recorded stack voltages are analyzed using a Wavelet Leader based Multifractal Analysis (WLMA) in order to identify their singularity spectra as fault signatures. This novel method based on leader discrete wavelet coefficients for the estimation of the singularity spectrum is a well-suited technique for non-stationary and non-linear signals.
- A feature selection method is used to select the most relevant singularity features and to remove the redundant ones.
- The selected singularity features are classified using Support Vector Machine and K-Nearest Neighbors techniques according to the considered operating situations (faults and combinations of faults).
Our results show that the proposed PEMFC diagnosis tool allows identifying simple operating failure cases and even more complicated situations that contain several failure types.

Keywords: Diagnostic, Fault Classification, Fractals, Fuel Cells, PEMFC, Singularity Analysis, Wavelet Leaders.

1 Introduction and Motivation
In the era of renewable and clean energies, the Fuel Cell (FC) technology gradually imposes its developments and applications in a wide spectrum of fields [1-3]. The fault detection and the diagnosis of FC stacks are obviously of prime importance when FC assemblies constitute the new key device of the emerging energy converter systems. Therefore, over the years, the level of requirements for the FC safety and reliability increases leading therefore to systematic automations and controls, to efficient monitoring and fault diagnosis processes able to optimize the performances, the availability and the durability of the complete generator. The performance of a diagnostic module used inside an energy converter system can be related with its capability to identify and isolate some failures before the equipment damage. After the fault identification step, the task of supervision triggers some alarms for manual maintenance procedures or for automatic actions in order to correct

the failure. A reliable diagnostic module allows a greater safety to avoid accidents, an increase of production by reducing the downtime of the system, and an increase of its lifetime. To these ends, recent researches have focused on the development of relevant techniques for FCs diagnostic [4, 5]. Among these techniques, the data-driven techniques [6, 7] attract more and more attention due to their relative simplicity of implementation and because they take advantage from efficient signal processing methods such as: Fourier transform, Wavelets transform, pattern recognition methods, etc. The method we have chosen is based on the pointwise singularity analysis of the FC stack voltage which is a typical non-linear signal. Actually, it is reasonable to assume that the operation of a FC under severe conditions affects the morphology of its voltage. The analysis of its local fluctuations can therefore provide direct information on the dynamics of the device and on its state-of-health as well. To perform a right characterization of these complex signals, some appropriate and robust techniques are obviously necessary.

In our study, we adopt the multifractal analysis of voltage signals based on wavelet leaders [8] in order to extract some latent information hidden in the singularity features and then to identify the signature of singularities for different fault operations. Indeed, the multifractal features can fully display the distribution of signal singularities, while the geometric characteristics and the local scaling behaviors are described more precisely [9]. The principle of the multifractal formalism consists to calculate two sets of coefficients associated to the signal: the Hölder exponent (h), that quantifies the local regularity strength of the signal and the Hausdorff dimension ($D(h)$) that associates each group of points with the same regularity strength to a non-Euclidean dimension. The graph $h \rightarrow D(h)$ provides a Singularity Spectrum (SS). Since the 80s, the research field of fractals has been the subject of several methods to compute the SS of natural and physical signals. The first pioneers in the development of this research are Stanley and Ostrowsky [10], and Pietronero and Tosatti [11]. The SS is intimately related with the generalized dimensions based on the box-counting or entropy techniques on which Grassberger and Procaccia have published widely [12, 13]. Besides, Peng and co-workers have proposed another method named, "Detrended Fluctuations Analysis" (DFA) [14]. Some years later, the wave-like oscillation named wavelet has been introduced to improve the SS estimation; Arneodo and his collaborators have developed the so-called "Wavelet Transform Modulus Maxima Method" (WTMM), which is based on the continuous wavelet transform of the signal [15]. Lashermes and Jaffard introduced the novel use of the Wavelet Leaders coefficients in the multiresolution scheme to address the same objectives [16].

In the literature, several studies have provided some comparisons, in terms of precision and computation cost, between different techniques that enable the SS determination [17, 18]. It has been shown theoretically and numerically that the formalism based on wavelet leaders allows an accurate computing of the SS for a wide variety of functions and random processes. The formalism presents multiple advantages: it is notably faster than other techniques; it can be easily implemented in dimension greater than 1 (e.g. for image processing) [19]. It has been successfully used in texture classification [20, 21], analysis of heart rate variability [22], fMRI (functional Magnetic Resonance Imaging) time series [23], and electrocardiogram signal [24].

This work is devoted to the development of a non-intrusive and on-line PEMFC diagnostic tool based on the observation of the stack voltage, and on the application of the wavelet leader based multifractal formalism to this signal. The test data are obtained by operating a PEMFC stack in various conditions corresponding to different fault scenarios; more details about the experimental and the set of recorded stack voltages will be given in Part 2. The theoretical basis of the "Wavelet Leaders based Multifractal Analysis" (WLMA) will be outlined in Section 3. The obtained multifractal features will be presented in Part 4 as well as the selection of the most pertinent ones that will be used to discriminate the different operating scenarios of the FC. The results (expressed in terms of good classification rates) obtained through different pattern recognition methods will be discussed, and a real-time implementation of the diagnosis procedure will be proposed at the end of the article. Finally, this paper will be completed with major conclusions.

2 Experimentation and Stack Voltage Data

The experimented FC is an 8 cell PEMFC stack manufactured by CEA LITEN in Grenoble, France. It has been designed for automotive applications and it is made of metallic gas distributor plates. The electrode active surface is 220 cm^2 and the nominal current I is 110A (nominal current density of 0.5 A cm^{-2}). The PEMFC stack was operated under a variety of scenarios using a 1 kW test bench developed "in-house" on the FC test platform of Belfort, France. The monitoring and controls of the FC test bench parameters are done using National Instruments (NI) materials and through a friendly Human-Machine Interface (HMI) also developed in-lab using Labview software.

The various fault scenarios considered have been introduced by changing different parameter values (namely: cathode stoichiometry rate '*FSC*', anode stoichiometry rate '*FSA*', gas pressure '*P*', cooling circuit temperature '*T*', and carbon monoxide 'CO' poisoning at the anode side) from the nominal ones. The data sets used in this study do not only contain different single operating faults of the FCs; they also consist of fault mixtures (i.e. combination of single fault scenarios). More details on the complete set of faults scenarios explored in this work are summarized in Tables 1 and 2.

Some examples of voltage stack signals recorded during various operating conditions corresponding to different fault scenarios are displayed in Fig. 1.

As we can see in Fig. 1, each operating condition induces an irregularity signature in the FC voltage signal. This observation motivated us to exploit the singularity analysis of the voltage in order to extract some relevant features that characterize its morphology efficiently. The method adopted to compute a multifractal SS is described in the following Section.

3 Wavelet Leaders Based Multifractal Features

3.1 Definition of Wavelet Leaders

Recently, a new formalism called *wavelets leaders* was built from the discrete wavelet transform. Its mathematical basis can be described as follow. Let a function $\psi(t)$ with a compact time support, called *mother-wavelet* [8] which satisfies the condition: $\int_R t^i \psi(t)dt \neq 0$, where $i = 0, 1, \dots, N_\psi - 1$ and the vanishing moment $N_\psi \geq 1$. So, a family of wavelets $\psi^i(t)$ can be generated; it is sometimes called *daughter-wavelets*.

The templates of $\psi(t)$ dilated to scales 2^j and translated to time positions $2^j k$ where j is the multiresolution parameter, with an orthonormal basis of $L^2(R)$, can be formulated as follow [8] [25]:

$$\psi_{j,k}(t) = \frac{1}{2^j}\psi\left(\frac{t-2^j k}{2^j}\right), j \in \mathbb{Z} \text{ and } k \in \mathbb{Z} \quad (1)$$

Then, the discrete wavelet transform of a signal $X(t)$ is defined by the following formula [25]:

$$d_X(j,k) = \int_R X(t)2^{-j}\psi\left(2^{-j}t - k\right)dt \quad (2)$$

Assuming the dyadic interval λ and the dyadic cube Γ [8] [25]:

$$\lambda = \left[k.2^j, (k+1).2^j\right] \quad (3)$$

$$\Gamma = 3\lambda = \lambda_{j,k-1} \cup \lambda_{j,k} \cup \lambda_{j,k+1} \quad (4)$$

Γ denotes the union of the interval λ with its two adjacent dyadic intervals [8]. Therefore, the *wavelet leader* is the local supremum of the wavelet coefficients located in the dyadic cube over all finer scales [25]:

$$L_X(j,k) = \sup_{\lambda' \subset \Gamma}\left|d_{X,\lambda'}\right| \quad (5)$$

The formula (5) indicates that to compute $L_X(j,k)$, which consists of the largest wavelet coefficient $d_X(j',k')$, we consider the indexes $(k-1)2^j \leq 2^{j'}k' < (k+2)2^j$ at all finer scales $2^{j'} \leq 2^j$. A possible scheme illustrating this definition is given in Fig. 2 [8] [23].

3.2 Wavelet Leaders based Multifractal Features Extraction

The purpose of multifractal analysis (or singularity analysis) is to study some signals whose pointwise Hölder regularity may change widely from point to point. This characterization is obtained by analyzing the behavior of structure functions, based on the discrete or continuous wavelets transform

with WLMA and WTMM methods respectively, in the limit of small scales. Let us define the structure functions $S_L(q,j)$, which quantify the spatial average of wavelet coefficients at a given scale 2^j :

$$S_L(q,j) = \frac{1}{n_j}\sum_{k=1}^{n_j}|L_X(j,k)|^q \quad (6)$$

Where q is the order of the statistical moment, $n_j \approx n / 2^j$ is the number of leaders available at each scale, and n the length of the sample [8].

The multifractal formalism consists in evaluating the behavior of the logarithm of structure functions in the limit of fine scales; this characterization [16] is given by the scaling exponents $\xi_L(q)$:

$$\xi_L(q) = \lim_{j\to 0} \inf \left(\frac{\log_2 S_L(q,j)}{j}\right) \quad (7)$$

In other terms, the structure functions $S_L(q,j)$ exhibit a power law behavior with respect to the scale analysis, in the limit of fine scales [16], and where C_q is a constant:

$$S_L(q,j) \cong C_q 2^{j\xi_L(q)} \quad (8)$$

The SS representing the function $h \to D(h)$ is obtained by the Legendre transform of the scaling exponents:

$$D_q(h) = \inf_{q\neq 0}(1 + qh - \xi_L(q)) \quad (9)$$

3.3 Related Parameters Selection

3.3.1 *Analyzing Wavelet and Vanishing Moments*

The most irregular voltage signal is observed when the *FSC* faults are introduced, and the impact demonstrates that longer impulses are added on the signal support (see Fig. 1). As for the multifractal analysis, the vanishing moment should be larger than the largest singularity exponent. Moreover, the overlarge vanishing moment will introduce some border effects. Therefore, the reasonable analyzing wavelet is selected as Daubechies 3 ('Db3') function (with 3 vanishing moments) [26, 27].

3.3.2 *Rang of q-Order Statistical Moments*

Let us consider the concept of the Hölder exponent. A positive exponent indicates that the function is continuous and has a given number of derivatives. A negative exponent implies that the function encloses transitions, jumps and eventually divergences to infinity. As the last characteristics are not observed in the studied voltage signals, we must avoid all negative values of h and $D(h)$.

To obtain the $D(h)$ entire curve by the Legendre transform, both positive and negative values of q-order are needed: $q \in [q^-, q^+]$. Note that $q = q^-$ and $q = q^+$ amplify the small and large fluctuations of the signal.

In this study, both q^- and q^+ are selected to avoid the negative values of the Hölder exponent h and Hausdorff dimension $D(h)$. So, in the case of our study: $q \in [-4, +5]$.

4 Results

We assess the performance of the proposed SS estimation procedure by applying it to the investigated PEMFC stack voltages acquired under the 10 operating conditions described in Section 2 (nominal conditions, 5 operating scenarios with one fault at a time, and 4 ones with 2 or 3 faults simultaneously). In this aim, we use 30 voltage profiles acquired for each operating scenario; each voltage profile covers 1000 points acquired at a frequency f_a =11Hz using the monitoring data system of the FC experimental test bench. The acquisition frequency was selected according to the technical possibilities offered by the test bench hardware used during the experimental campaign carried out with the 8 cell PEMFC stack. The window size of the analyzed signal was chosen to have enough SS for the classification step and to make the wavelet analysis possible (i.e. to have less side-lobe effects due to the wavelet transform [28]).

4.1 Obtained Multifractal Features

The multifractal features can fully display the distribution of the signal singularities. The geometric characteristics and the local scaling behaviors are described precisely. When the operating conditions of the FC are changed according to the different fault scenarios, the singularities distribution of the stack voltage is different from the nominal conditions. The average SS computed using WLMA and related with the various faults shown in Fig. 1 are plotted in Fig. 3.

As we can see at first sight, each operating fault gives its own stamp on the morphology of the stack voltage. This behavior is revealed by the shape and the location of the corresponding singularity spectra (Fig 3(a) and (b)). So, when the obtained SS is shifted to the left, that means a high irregularity of the voltage signal and conversely, when shifted to the right that reveals a more regular signal.

On the one hand, the voltage signals associated to the FSC fault (single fault or combination of fault conditions) contain sharp and impulsive variations (Fig. 1) with relatively close magnitudes. This behavior is established by reduced singularity spectra (tiny concave arcs) and a high irregularity (Fig .3). On the other hand, large spectra are obtained with the *FSA* and Pressure voltage faults, which reveal the presence of several fluctuations sets with various magnitudes on the voltage signals.

Based on these results, the classification of the obtained multifractal features is done in the next subsection.

4.2 Results of Multifractal Features Classification

To improve the performance of the fault classification method, it is recommended to select the most relevant features. Moreover, this task allows the reducing of the computational complexity. In our study, we use the Minimum Redundancy – Maximum Relevance (MRMR) technique. The MRMR feature selection technique was recently introduced for gene selection application [29]. This method selects the features according to their relevance to the concerned target and the redundancy among the features themselves. More details on this technique can be found in [29-31]. The MRMR selected singularity features are then classified using the pattern recognition methods named Support Vector Machines (SVM) and K-Nearest Neighbours (KNN).

Actually, 20 SS per class are used to generate the learning database and the 10 others serve as test data to evaluate the performances of both SVM and KNN methods. Each SS contains 28 features (19 h data and 19 $D(h)$ data). The number of the SS features is governed by a q-order interval: from q^-=-4 with a step of 0.5 to q^+=+5, we obtain 19 Hölder exponents and 19 Hausdorff dimensions. When all the 28 multifractal features are introduced in the diagnosis algorithm, the classification rates obtained are equal to 83,42 % for the KNN method and 82.63% for the SVM classifier.

So, by applying the MRMR method on the full feature set (28 features) of the SS, the good classification rate obtained with the SVM classifier using the top 13 selected features is about 84.42%, against 85.71% obtained by the KNN method with 8 selecting optimal features.

Besides, limiting the application of the MRMR technique only on the Hölder exponents (h features) leads to better results in terms of good classification rates, both for SVM and KNN. Indeed, the SVM classifier offers 85.71% of good classification rate with 15 selected h features and the computing time is about 350 ms. The best classification rate obtained by KNN is equal to 89.61% when only 6 optimal features are selected among 19 h features, with a fast computing time of about 4 ms (Fig. 4).

The confusion matrix of the best results obtained on each class is shown in Table 3. As we can see, despite a significant number of classes and samples to distinguish, the proposed diagnosis strategy identifies successfully several complex operating faults.

Thus, the combination of the MRMR technique with the KNN classifier by using only the Hölder exponent features offers the best discrimination between the 10 classes described previously. We can conclude that the punctual singularity strengths of the stack voltage reveal very useful information on the physical and electrochemical phenomena involved inside the FC.

4.3 Real Time Implementation of the WLMA Diagnosis Method

In order to perform the real time diagnosis operation, the FC test bench is connected to a Personal Computer with the following characteristics: Intel ® Core ™ i7-2960 XM, CPU @ 2.7 GHz, RAM: 16 GO. During the PEMFC operation, the stack voltage data are recorded with an acquisition frequency of 11 Hz through the Labview interface of the FC test bench and shared using an internet link with a Matlab code that calculates the SS with the Personal Computer (Fig. 5). Then, the SS data are sent back to the testbench and the spectrum can be displayed on the HMI. The time cost of a full SS (28 features) computation is about 0.7 s. The MRMR technique reduces the computing time to 0.15 s. Finally, the feature vector is assigned using the KNN classifier to the class of the sample that is the nearest one in the training database.

5 Conclusions

The proposed diagnostic strategy dedicated to the determination and monitoring of the FC state-of-health allows achieving three main objectives. The first objective concerns the possibility of detecting a wide range of FC faults, including the most complex situations (combination of faults). The second aim is to limit the instrumentation needed for the diagnosis task (non-intrusive method based on the one and only stack voltage measurement). The latter is the possibility to operate in real-time mode (on-line method), leading to the outlook of a possible feedback on the FC control-command. The first objective is achieved by the powerful discrimination of the wavelet leader features. The diagnosis task is done by the observation of the "free" stack voltage evolution. No additional current or voltage solicitation needs to be applied as it is the case for Electrochemical Impedance Spectroscopy measurement for instance. The interesting computing time costs of the wavelet leaders and KNN classifier makes possible the future implementation of the algorithm on embedded technologies that could equip some real FC application systems.

Acknowledgments

The French National Research Agency (ANR) is gratefully acknowledged for its support through the funding of the DIAPASON2 project.

References

[1] M. Thoennes, A. Busse and L. Eckstein, *Fuel Cells* **2014**, 6, 781-791.
[2] J. Hall., *Fuel Cells* **2014**, 6, 945-953.
[3] J-K Kuo, J-J Hwang and C-H Lin, *Fuel Cells* **2012**, 6, 1104-1114.
[4] N. Yousfi Steiner, D. Hissel, P. Moçotéguy, D. Candusso, D. Marra, C. Pianese and M. Sorentino, *Fuel Cells* **2012**,2, 302-309.
[5] D. Hissel, D. Candusso, F. Harel, *IEEE Trans. Vehicular Technology* **2007**, 56, 2414-2420.
[6] N. Yousfi Steiner, D. Hissel, P. Moçotéguy, D. Candusso, *Int. Journal of Hydrogen Energy* **201**1, 36, 3067-3075.
[7] D. Benouioua Ait Aouit, D. Candusso, F. Harel, L. Oukhellou, *Int. Journal of Hydrogen Energy* **2014**, 39, 2236-2245.
[8] W. Herwig, P. Abry, *IEEE Transactions on Signal Processing* **2007**, 55, 4811 – 4820.
[9] R. Lopes,N. Betrouni, *Medical Image Analysis* **2009**, 13, 634-649.
[10] G. Stanley, N. Ostrowsky, *Fractal and Non-Fractal Patterns in Physics*, In On Growth and Form, Springer Netherlands Publisher, **1986**, pp. 310.
[11] L. Pietronero, E. Tosatti, *Fractals in Physics*, North-Holland, Amsterdam, **1986**.
[12] P. Grassberge, *Journal of Statistical Physics*, **1981**, 26, 173-179.
[13] P. Grassberger, *Estimating the fractal dimensions and entropies of strange attractors*, *Chaos*. Edited by Arun. V. Holden. Published by Manchester University Press. **1986**, 291-311.
[14] C.K. Peng, S.V. Buldyrev, S. Havlin, M. Simons, H.E. Stanley, A. L. Goldberger, *Physical Review E* **1994**, 49, 1685-1689.
[15] A. Arneodo, F. Argoul, J.F. Muzy, M. Tabard, E. Bacry, *Fractals* **1993**, 1, 629-649.

[16] B. Lasherms, S. Jaffard, P. Abry, *Proc. IEEE International Conference on Acoustics, Speech and Signal Processing, ICASSP* **2005**, 4, 161-164.
[17] E. Serrano, A. Figliola, *Physica A: Statistical Mechanics and its Applications* **2009**, 388, 2793-2805.
[18] J. W. Kantelhardt, Fractal and multifractal time series, in: Mathematics of Complexity and Dynamical Systems, Springer (Ed.), Editor Robert A. Meyers, California, **2011**, pp. 463-487.
[19] H. Wendt, S. Roux, S. Jaffard, P. Abry, *Signal Processing* **2009**; 89, 1100-1114.
[20] H. Wendt, P. Abry, S. Jaffard, H. Ji, Z. Shen, *Proc. 16th IEEE Int. Conf. on Image Processing, ICIP* **2009**, 3785–3788.
[21] Y. Xu, X. Yang, H. Ling, H. Ji, *IEEE Conf. on Computer Vision and Pattern Recognition* **2010**, 161-168.
[22] P. Abry et al, *Proc. Annual Int. Conf. of the IEEE Engineering in Medicine and Biology Society, EMBC* **2010**, 106–109.
[23] P. Ciuciu, P. Abry, C. Rabrait, H. Wendt, *IEEE Journal on Selected Topics in Signal Processing* **2008**, 2, 929-943.
[24] P. Abry et al, *Proc. IEEE International Conference on Acoustics, Speech and Signal Processing, ICASSP* **2010**, 566–569.
[25] S. Jaffard, B. Lashermes, P. Abry, *Wavelet leaders in multifractal analysis, in Wavelet Analysis and Applications*, Birkhäuser Verlag (Ed.) **2006**, pp. 219-264.
[26] W. Uhm, S. Kim, *Journal of the Korean Physical Society* **1997**, 32, 1-7.
[27] S. Jaffard, C. Melot, R. Leonarduzzi, H. Wendt, P. Abry, S-G. Roux, M-E. Torres, *Physica A* **2016**, 448, 300-318.
[28] A. Ouahabi, *Analyse multirésolution pour le signal et l'image*, Lavoisier (Ed). **2012**, pp. 338.
[29] H. Peng, F. Long, C. Ding, *IEEE Trans. on Pattern Analysis and Machine Intelligence* **2005**, 27, 1226-1238.
[30] C. Ding, H. Peng, *Journal of Bioinformatics and Computational Biology* **2005**, 3, 185-205.
[31] Hanchuan Peng's web site. Information on MRMR (Minimum Redundancy Maximum Relevance Feature Selection). http://penglab.janelia.org/proj/mRMR/. **2014**.

Figures

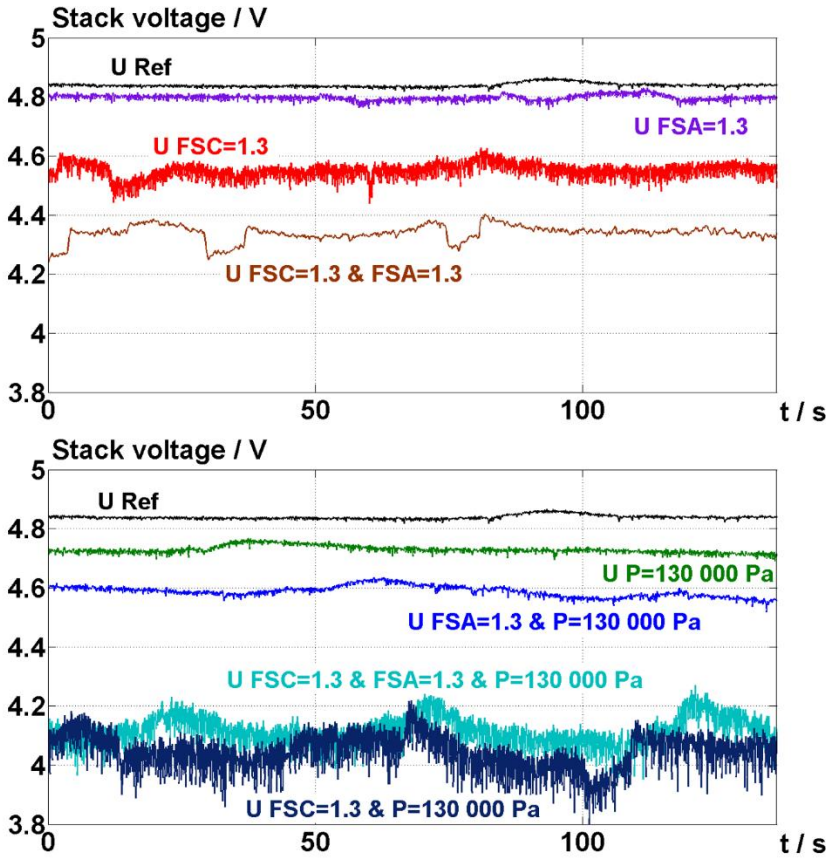

Figure 1: Examples of PEMFC stack voltages (U) *vs*. time acquired in different operating conditions.

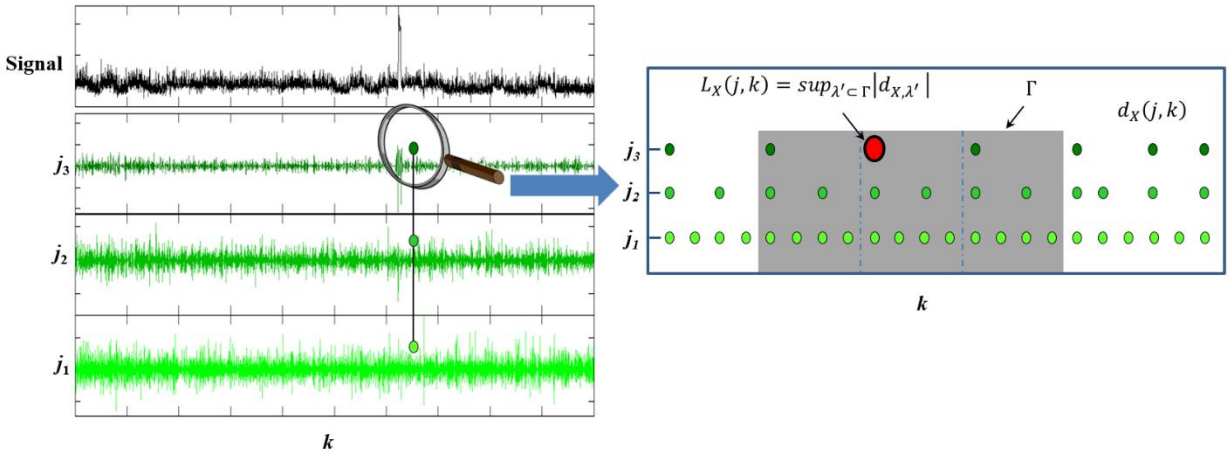

Figure 2: Left: example of a voltage signal decomposition using the Daubechies wavelet 'db3'. Right: a zoom in on the obtained wavelet coefficient details to give an illustration of the principle used in tracking the wavelet leaders L_X (red circle). These last ones are calculated from the discrete wavelet coefficients $d_X(j,k)$ (green dots) by taking the supremum in the time neighborhood $\Gamma = 3\lambda$ over all finer scales $2^{j'} < 2^j$ (area in grey).

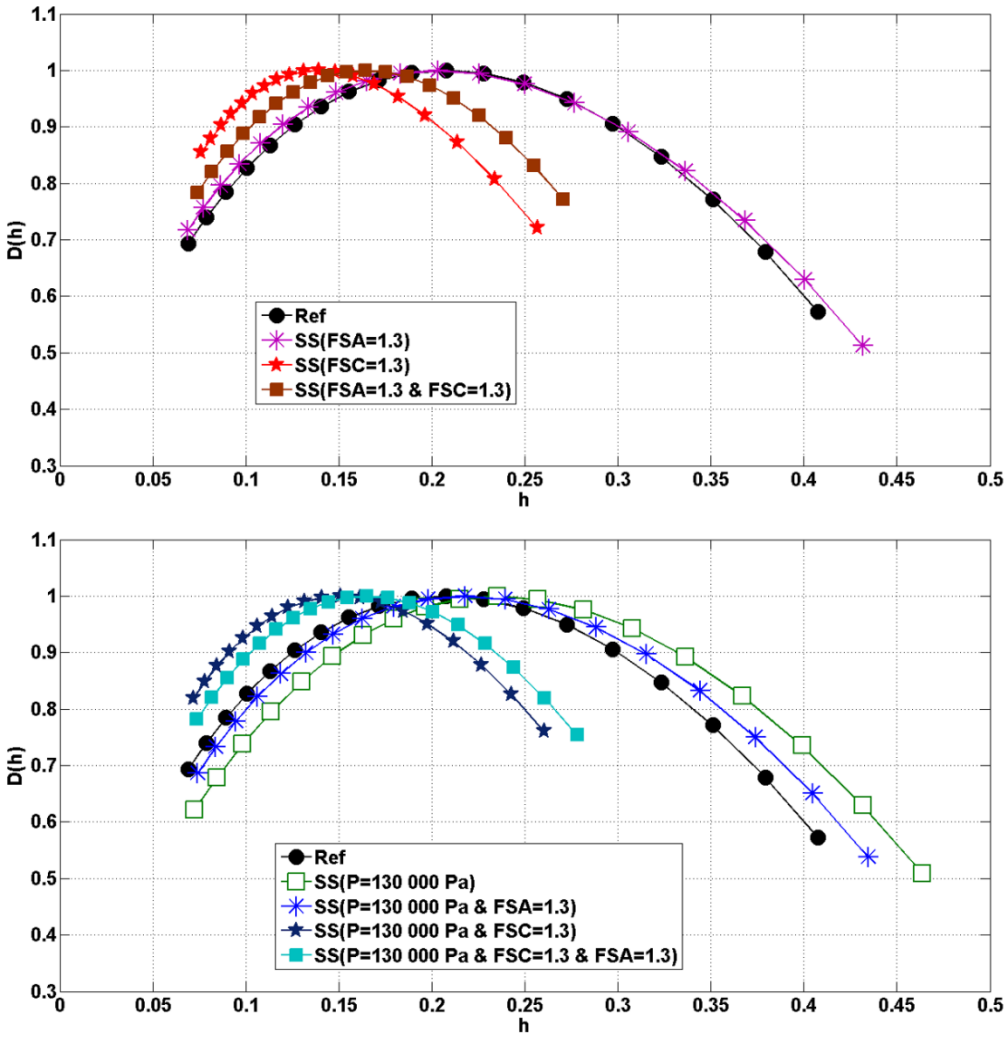

Figure 3: Average Singularity Spectra (SS) computed on 30 signals /operating conditions related with the different faults exhibited in Fig. 1.

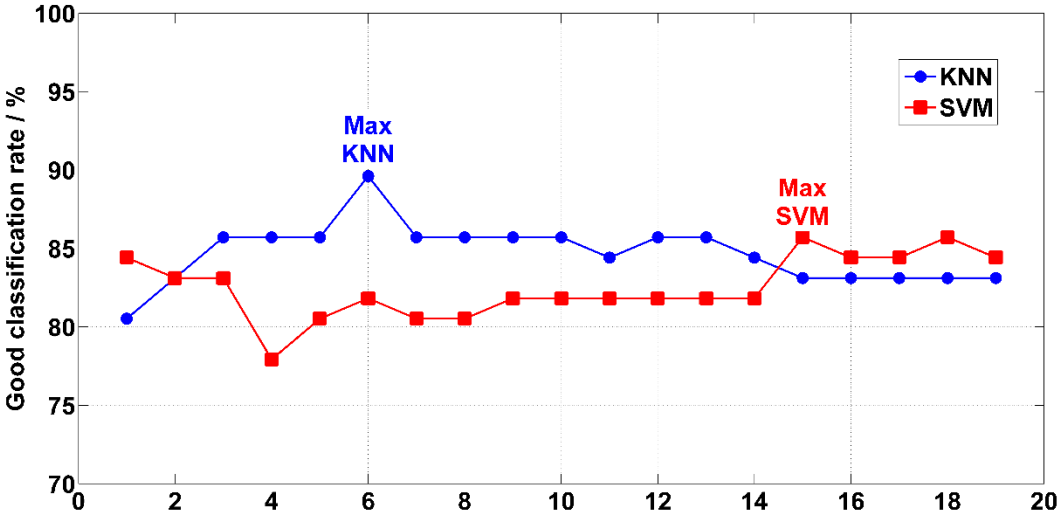

Figure 4: The wrapper selection / classification results on the Hölder exponents (*h* features).

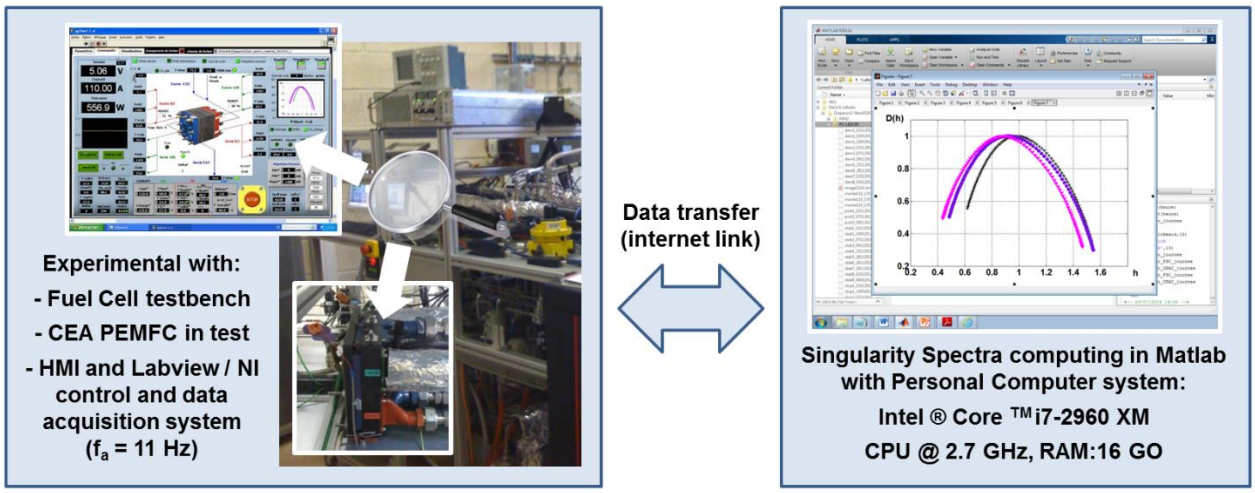

Figure 5: The different devices used for the on-line implementation of the PEMFC diagnosis strategy.

Tables

Table 1: The set of single fault scenarios applied during the experimentation with I = 110 A.

Parameters value	Nominal conditions (Ref)	Cathode flow fault (DFSC)	Anode flow fault (DFSA)	Inlet gas pressures fault (DP)	Cooling circuit temperature fault (DT)	CO poisoning (DCO)
FSC	2	**1.3**	2	2	2	2
FSA	1.5	1.5	**1.3**	1.5	1.5	1.5
P, Pa	1.5×10^5	1.5×10^5	1.5×10^5	**1.3×10^5**	1.5×10^5	1.5×10^5
T, C	80	80	80	80	**75**	80
Presence of CO, ppm	0	0	0	0	0	**10**

Table 2: The set of fault combination scenarios applied during the experimentation with I = 110 A.

Parameters value	Nominal conditions (Ref)	Both cathode flow and pressure faults (DFSC & DP)	Both anode flow and pressure faults (DFSA & DP)	Both anode and cathode flow faults (DFSC & DFSA)	Anode and cathode flow faults and pressure fault (DFSC & DFSA & DP)
FSC	2	**1.3**	2	**1.3**	**1.3**
FSA	1.5	1.5	**1.3**	**1.3**	**1.3**
P, Pa	1.5×10^5	**1.3×10^5**	1.3×10^5	1.5×10^5	**1.3×10^5**

Table: 3 Confusion matrix of the good classification rates %, obtained with MRMR and KNN.

Class	C_0	C_1	C_2	C_3	C_4	C_5	C_6	C_7	C_8	C_9
Ref	**87.5**	0	0	12.5	0	0	0	0	0	0
DFSC	0	**100**	0	0	0	0	0	0	0	0
DFSA	0	0	**100**	0	0	0	0	0	0	0
DP	50	0	0	**50**	0	0	0	0	0	0
DT	0	0	0	0	**100**	0	0	0	0	0
DCO	0	0	0	0	0	**100**	0	0	0	0
DFSC & DP	0	0	0	0	0	0	**100**	0	0	0
DFSA & DP	0	0	0	0	0	0	0	**71.43**	28.57	0
DFSC & DFSA	0	0	0	0	0	0	0	0	**100**	0
DFSC & DFSA & DP	0	0	0	0	0	0	0	0	0	**100**

With: $C_0 \equiv \widehat{Ref}, C_1 \equiv \widehat{DFSC}, C_2 \equiv \widehat{DFSA}, C_3 \equiv \widehat{DP}, C_4 \equiv \widehat{DT}, C_5 \equiv \widehat{DCO}, C_6 \equiv \widehat{DFCS\ \&\ DP}$,
$C_7 \equiv \widehat{DFSA\ \&\ DP}, C_8 \equiv \widehat{DFSC\ \&\ DFSA}, C_9 \equiv DFSC\ \&\ \widehat{DFSA\ \&\ DP}$